The long-term cement studies project: the UK contribution to model development and testing

C. E. Watson[1],*, D. Savage[2], J. Wilson[1], C. Walker[3] and S. J. Benbow[1]

[1] Quintessa, The Hub, 14 Station Road, Henley-on-Thames, Oxfordshire RG9 1AY, UK
[2] Savage Earth Associates, 32 St Alban's Avenue, Queen's Park, Bournemouth, Dorset BH8 9EE, UK
[3] JAEA, Tokai-mura, Naka-gun, Ibaraki-ken 319-1194, Japan

ABSTRACT

The international long-term cement studies (LCS) project aims to increase the understanding of the behaviour of cement within a radioactive waste disposal system and how hyper-alkaline leachates may interact with host rock. Such an understanding enables confident, robust and safety-relevant statements to be made concerning future system behaviour, irrespective of host rock, engineered barrier system, or waste type. The LCS project involves laboratory experiments, *in situ* tests and numerical modelling to address these issues. The agencies participating are Nagra (Switzerland), JAEA (Japan), the Nuclear Decommissioning Authority, Radioactive Waste Mangement Directorate (UK), Posiva (Finland) and SKB (Sweden).

Project activities have included: the development of conceptual and theoretical models of cement−rock interaction; testing of numerical models against data from laboratory experiments and industrial and natural analogues of cement−rock reaction; and the synthesis and incorporation of performance assessment (PA) relevant data from analogue studies. Key threads running through these studies include an analysis of issues relating to upscaling of processes and data to the greater temporal and spatial scales relevant to PA, and investigations of modelling the changes in physical properties that accompany geochemical reaction. Here we present examples of the results from model test cases, highlighting the important issues that have arisen.

Introduction

In a number of concepts for a geological disposal facility (GDF) for radioactive waste, cement-based materials are used for mechanical support, backfilling of cavities, grouting of fractures in the host rock, and/or immobilization of radionuclides in waste forms (e.g. Gribi *et al.*, 2008). Chemical reactions may occur within these materials which could potentially lead to a loss of their containment properties due to mineral alteration and related changes in swelling capacity, hydrogeological properties (porosity and permeability) and

sorption properties. Within the host rock it is expected that there would be a net decrease in porosity and permeability as fractures become filled with new relatively high-volume minerals.

The international collaborative long-term cement studies (LCS) project, a partnership between Posiva (Finland), JAEA (Japan), the Nuclear Decommissioning Authority (NDA) (UK), SKB (Sweden) and Nagra (Switzerland), aims to further understanding in this area by conducting *in situ* field experiments with more realistic boundary conditions and longer time-scales than have previously been achieved. The experimental work is informed by modelling studies, both of the field experiments and of other published work. Consideration is also given

* E-mail: clairewatson@quintessa.org

to alternative materials to Portland cement, such as low-pH cement blends, the use of which may help to mitigate potential problems caused by hyper-alkaline leachates. The LCS project has been active since 2006, building upon the work of the HPF (hyperalkaline plume in fractured rock) project (e.g. Soler *et al.*, 2004), and will continue until at least 2013.

The current paper is concerned with the modelling studies carried out within the LCS project. Two preliminary code intercomparison exercises have been carried out (Savage *et al.*, 2011), involving modelling cement hydration experiments (Lothenbach and Winnefeld, 2006), and a short-term column laboratory experiment where high-pH liquid was advected through a fracture in a column of granite rock (Soler and Mäder, 2007). These modelling exercises showed that the dominant reaction pathways are fairly well understood but some significant differences existed amongst the precise parameterization (e.g. reactive surface areas, dependencies of rate on pH, types of secondary minerals) and, in some instances, the processes involved (e.g. partition of alkali elements between solids and liquids during cement hydration, kinetic models).

The LCS project realizes the importance of studying natural/industrial analogues to build confidence in our models and understanding of hyperalkaline systems. Two such cases have been investigated; the Maqarin natural analogue in Jordan, where naturally high-pH waters (pH >12) flow through a fractured biomicritic limestone (e.g. Smellie *et al.*, 2001), and the Tournemire industrial analogue in France, where cement-filled boreholes have been in contact with a mudrock for over 15 years (Tinseau *et al.*, 2006). The Maqarin modelling work is currently ongoing, but the Tournemire work is summarized in the remainder of the current paper.

The Tournemire industrial analogue

Located on the southern border of the French Massif Central region, the Tournemire experimental platform is based around a tunnel built between 1882 and 1886 and several galleries which have been excavated since 2003 through Jurassic marls and mudstones. It now forms the core of a research programme studying the interaction of mudstones with cementitious materials, conducted by the Institute for Radioprotection and Nuclear Safety (IRSN) and the Scientific Research National Centre (CNRS).

In the 1990s, exploration boreholes were drilled into the basement of the tunnel and subsequently filled with cement and then concrete, which have been in contact with the mudstone for 15−20 years. These boreholes have since been overcored and mineralogical characterization has been performed (Tinseau *et al.*, 2006; Techer *et al.*, 2012). The samples of interest for the present study come from the middle part of the borehole (at a depth of ~1.55 m from the tunnel floor), which was water saturated and isolated from the atmosphere once sealed. The mudstone was locally damaged during the original borehole coring process, resulting in small fractures that radiate from the concrete interface into the argillite matrix. These fractures are less than a millimetre wide and extend a few centimetres into the matrix.

Reaction fronts are clearly visible in cross-sections removed from the sample (Tinseau *et al.*, 2006; De Windt *et al.*, 2008), with changes in the texture and mineralogy observed at distances of approximately 1 cm from the concrete contact in the case of the undisturbed mudstone, and 1−2 cm when a fracture was present. Beyond this the mudstone matrix is largely undisturbed. Detailed analysis revealed three distinct front zones within the mudstone (Fig. 1) as follows. (1) The first few millimetres around the concrete/mudstone interface are characterized by the precipitation of calcium carbonate polymorphs (vaterite, aragonite and calcite), gypsum and ettringite, and the dissolution of the clay and quartz contents of the mudstone. There is a corresponding decrease in porosity in this section of the mudstone. (2) A second centimetre-scale zone is characterized by calcite precipitation and honeycombed neoformed clay-like phases with the presence of calcium aluminosilicate hydrate (C-A-S-H) and calcium silicate hydrate (C-S-H) phases with high Si content. (3) In a third centimetre-scale zone, more calcite precipitation is observed, with possible potassium feldspar overgrowths. The first stage of mineralogical study (Tinseau *et al.*, 2006) suggested the presence of Na-zeolites in this third zone, though later studies (Techer *et al.*, 2012) have not confirmed this observation. Within the concrete an increase in porosity is observed near the interface, with a corresponding decrease in the portlandite content. There is also an increase in the amount of C-S-H gel, calcite and ettringite present.
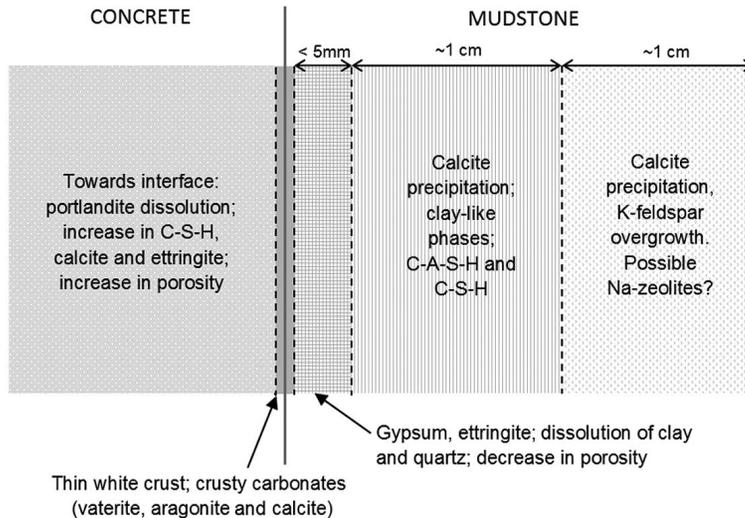
FIG. 1. Summary of the main mineralogical changes observed in samples taken from the Tournemire site (based on the findings of Tinseau *et al.*, 2006).

Modelling Tournemire

Each of the modelling teams participating in the LCS project used their preferred computer codes and techniques to model the Tournemire analogue, with the aim that ideas could be shared and sensitivities to various assumptions explored. Here we summarize only the results of the Quintessa/NDA team, which have been reported fully by Watson *et al.* (2011).

The model is based upon that of De Windt *et al.* (2008) and was simulated in the current paper using the reactive transport module of the general-purpose modelling tool *QPAC* (e.g. Savage *et al.*, 2010; Watson *et al.*, 2011). This is based on a finite volume scheme and is capable of solving fully coupled non-linear reactive-transport problems. Although models of both intact and fractured mudstone were considered, the results presented here relate only to the intact mudstone case. A simplification is made by assuming that the borehole is filled homogeneously with concrete (i.e. the inner cement core is ignored), as it is the concrete/mudstone interface that is of interest. The temperature of the Tournemire site, and that used in the model, is 15ºC.

Transport properties

Within the matrix of the mudstone, porewater contents are very low (3−5 wt.%) and solute transport is substantially driven by diffusion. The effective diffusion coefficient of tritiated water (HTO) parallel to the argillite bedding was selected from previous measurements to be 2×10^{-11} m^2 s^{-1} for a porosity of 9.5 vol.% (De Windt *et al.*, 2008). Assuming non-porous aggregates and typical ordinary Portland cement (OPC) parameters, the effective diffusion coefficient and porosity of the concrete were estimated to be 3×10^{-12} m^2 s^{-1} and 13%, respectively.

The effect of changing porosity on diffusion was incorporated in the modelling using Archie's law:

$$D_e = \frac{D_p}{\theta^{1-m}} \quad (1)$$

where D_e is the effective diffusion coefficient (m^2 s^{-1}); D_p is the pore diffusion coefficient (m^2 s^{-1}); θ is the porosity (dimensionless); and m is a constant, here taken to be 2. Using the effective diffusion and porosity values (by volume) above this gives pore diffusion coefficients of 2.1×10^{-10} m^2 s^{-1} and 2.3×10^{-11} m^2 s^{-1} in the mudstone and the concrete, respectively.

Mudstone composition

The mudstone composition used in the model is listed in Table 1. Clays are the most abundant minerals and are composed mostly of kaolinite and 'illite' (pure illite and interstratified illite/

3447

TABLE 1. Composition and surface area data for mudstone (from De Windt *et al*., 2008).

Mineral	Wt.%	Vol.%	Surface area per gram of mineral (m^2 g^{-1})	Surface area per m^3 of mudstone (m^2 m^{-3})
Calcite	16.0	14.5	0.02	1.0×10^4
Dolomite	1.0	0.9	0.02	5.0×10^2
Muscovite (illite)	32.0	27.7	0.1	1.0×10^7
Kaolinite	6.5	6.1	0.1	5.0×10^6
K-feldspar	11.0	10.6	0.02	2.5×10^3
Montmorillonite	7.5	6.7	0.1	5.0×10^6
Quartz	26.0	24.0	0.02	1.0×10^4
Porosity	–	9.5	–	–

smectite with more than 70% of illite), smectite is present as a minor component. Detrital muscovite and K-feldspar have also been identified. In the model described here (and also as described by De Windt *et al*., 2008), montmorillonite represents the smectitic part of the mudstone, and muscovite is used as a proxy for illite. Calcite is the predominant carbonate and dolomite is present in a smaller proportion. Framboidal pyrite, which represents less than 1 wt.% of the mudstone, was not included by De Windt *et al.* (2008), and is also excluded from the present model.

The reactive surface areas of the various minerals were modified from those presented in De Windt *et al.* (2008) by decreasing the values for kaolinite, illite and montmorillonite to reflect 'edge' rather than 'total' surface areas [using data from Kline and Fogler (1981)] as shown in Table 1. In the absence of any reliable data for

individual minerals, the reactive surface areas of the secondary minerals were calculated assuming a sand-like grain size of 100 μm.

Concrete composition

Following De Windt *et al.* (2008), the phases in the concrete are shown in Table 2. Here we use monocarbonate in place of monosulfate, as preliminary calculations indicated that monosulfate would be rapidly converted to monocarbonate in the environmental conditions assumed. Thus, rather than explicitly modelling this, the conversion was assumed and the porewaters adjusted accordingly. An ideal solid solution is used to represent the C-S-H gel, based on the model developed by Kulik and Kersten (2001) and as redefined by Matschei *et al.* (2007) and Lothenbach *et al.* (2008), which uses tobermorite-like (C-S-H$_{Tob}$) and jennite-like

TABLE 2. Compositional and surface area data for concrete (based on that presented by De Windt *et al*., 2008).

Mineral	Wt.%	Vol.%	Surface area per gram of mineral (m^2 g^{-1})	Surface area per m^3 of mudstone (m^2 m^{-3})
Calcite (aggregate)	68.2	56.4	0.02	2.5×10^4
Portlandite	7.6	7.6	10	1.0×10^{-6}
C-S-H$_{Jen}$	20.2	18.5	10	1.0×10^7
C-S-H$_{Tob}$	0.4	0.4	10	1.0×10^7
SiO$_{2am}$	0	0	10	1.0×10^7
Ettringite	1.5	1.9	10	2.5×10^5
Hydrotalcite	0.5	0.5	10	5.0×10^4
Monocarbonate	1.5	1.6	10	2.5×10^5
Porosity	–	13.0	–	–

TABLE 3. Composition of concrete and mudstone pore waters at 15ºC (based on Beaucaire *et al*., 2008). Solubility constraints are indicated as appropriate.

Species	Molality (mol kg^{-1})	
	Concrete	Mudstone
pH	13.4	7.86 (calcite)
Na	5.00×10^{-2}	1.86×10^{-2}
K	1.10×10^{-1} (charge balance)	4.65×10^{-5} (illite)
Ca	2.72×10^{-3} (portlandite)	1.11×10^{-3}
Mg	9.82×10^{-11} (hydrotalcite)	9.00×10^{-4}
Si	1.07×10^{-4} (CSH_Jen)	1.20×10^{-4}
Al	2.15×10^{-5} (monocarbonate)	3.16×10^{-8} (kaolinite)
Cl	1.00×10^{-6}	6.37×10^{-3} (charge balance)
S	5.27×10^{-4} (ettringite)	6.76×10^{-3}
C	5.23×10^{-5} (calcite)	3.55×10^{-3}

(C-S-H$_{Jen}$) gel endmembers to represent molar Ca/Si ratios of 0.83 and 1.67, respectively.

Porewater composition

The initial porewater compositions of the concrete and mudstone are shown in Table 3 and are based on those described by Beaucaire *et al*. (2008). The mudstone porewater is of Na-Cl-(HCO$_3$) type, with a Cl$^-$ content around 10 mmol l^{-1} and pH close to 8. The main assumption associated with these compositions is that concentrations of some key components are controlled by the equilibrium solubility of minerals/solids present in the concrete and mudstone, rather than by ion exchange or other processes.

Mineral precipitation/dissolution

All minerals were assumed to precipitate/dissolve at a volumetric rate (mol m^{-3} s^{-1})

governed by the following rate equation (e.g. Lasaga, 1998):

$$\text{Rate} = Ak_0(a_{H^+})^n(\Omega - 1) \qquad (2)$$

where A is the mineral reactive surface area unit total volume (m^2 m^{-3}); k_0 is the kinetic rate (mol m^{-2} s^{-1}); a_{H^+} is the activity of H$^+$ in solution (dimensionless); n is a constant (dimensionless); and Ω is the reaction quotient given by the ion activity product (IAP) of the mineral divided by the equilibrium constant, K (dimensionless). A positive rate corresponds to precipitation, a negative rate to dissolution. Note that this leads to an asymmetric precipitation/dissolution rate (the range for the former is unbounded, whereas the latter is bounded in the range [−1, 0] as Ω is always positive), but due to a lack of reliable data in the literature, the same value of k_0 is adopted in both cases. This is consistent with the theory of detailed balancing (e.g. Lasaga, 1998).

TABLE 4. Kinetic data for primary minerals in the mudstone at 25ºC.

Mineral	$\log_{10}(k_0)$ (mol m^{-2} s^{-1})	n	Source
Calcite	−5.2	0	Busenberg and Plummer (1982)
Dolomite	−5.1	0	Palandri and Kharaka (2004)
Muscovite (illite)	−14.6	−0.22	Palandri and Kharaka (2004)
Kaolinite	−17.1	−0.472	Palandri and Kharaka (2004)
K-feldspar	−21.2	−0.823	Palandri and Kharaka (2004)
Montmorillonite	−13.6	−0.15	Sato *et al*. (2004)
Quartz	−16.3	−0.5	Palandri and Kharaka (2004)

Kinetic data for the primary mudstone minerals are listed in Table 4 and those for the secondary minerals are listed in Table 5. Activation energy data are not available for all minerals at 15ºC, so data quoted here are for a temperature of 25ºC. Cement minerals were allowed to dissolve at a uniform rate of 10^{-12} mol m^{-2} s^{-1} (e.g. Baur *et al.*, 2004). The kinetic rates employed (embodied by the form of the kinetic rate equation, the kinetic rate constant and the reactive mineral surface area assumed) are generally one of the greatest uncertainties in any geochemical model. However, particularly in diffusion-based systems, the transport of reactants is the limiting factor rather than the kinetic rate, resulting in uncertainties in the kinetic rates having a reduced impact. This has been investigated in the current study by including a variant case assuming larger reactive surface areas for the secondary minerals, which is not reported in detail here; further information can be found in Watson *et al.* (2011).

A wider range of secondary minerals than those considered by De Windt *et al.* (2008) was selected and include zeolites/feldspathoids (analcime, laumontite, gismondine, scolecite, stilbite, mordenite), brucite, gypsum and the calcium carbonate polymorph aragonite. As discussed previously, zeolites were originally identified by IRSN in their mineralogical investigations, but not subsequently confirmed (De Windt *et al.*, 2008). Secondary mineral surface areas were calculated by assuming spherical grains of diameter 100 μm or 3160 μm (the latter chosen to result in a surface area per grain approximately 1000 times larger than the former).

Thermodynamic data

The thermodynamic data used in the modelling were mainly chosen from the Lawrence Livermore (LLNL) database, '*thermo.com.V8.R6.230*', and calculated at 15ºC. Cement-phase data were mainly extracted from the compilations of Matschei *et al.* (2007) and Lothenbach *et al.* (2008) to give consistent equilibrium solution compositions at different temperatures. Full details of data used can be found in Watson *et al.* (2011).

Data for ion exchange in the mudstone were taken from Beaucaire *et al.* (2008), whereas those for clay edge site reactions were taken from Bradbury and Baeyens (2003).

Discretization and boundary conditions

The intact mudstone matrix was modelled using a 1D radial geometry, including both the concrete and the mudstone. A total of 46 finite volume compartments were applied to the concrete section (widths of 0.2−2.5 mm). Similarly, 145 compartments were used in the mudstone section (widths of 0.2−6 mm). Discretization was finest around the interface between the two materials. A coarser grid was also tested to investigate the effect of discretization on the model results; it was found that the mineralogy of the system at the end of the simulation was broadly the same in both cases. However, as with all geochemical models of this type, the exact timing of porosity clogging within a single compartment is dependent on the size of that compartment.

TABLE 5. Kinetic data for secondary minerals ($T = 25$ºC).

Mineral	$\log_{10}(k_0)$ (mol m^{-2} s^{-1})	n	Source
Analcime	−13.9	−0.4	Savage *et al.* (2001)
Aragonite	−5.5	0	Busenberg and Plummer (1982)
Brucite	−8.2	0	Palandri and Kharaka (2004)
Chalcedony	−14.5	−0.5	Plettinck *et al.* (1994)
Gismondine	−10.2	−0.02	as for scolecite
Gypsum	−2.8	0	Palandri and Kharaka (2004)
Laumontite	−12.3	0	Savage *et al.* (1993)
Mordenite	−10.2	−0.02	as for scolecite
Scolecite	−10.2	−0.02	Mao (2010)
Sepiolite	−8.2	0	as for brucite
Stilbite	−10.2	−0.02	as for scolecite
Vaterite	−5.5	0	as for aragonite

A constant concentration boundary condition was applied to the outer mudstone boundary (at r = 50 cm), using the initial mudstone porewater as given in Table 3. Symmetry arguments allow all other boundaries to be closed.

Sensitivity analysis

A number of variant cases were run to investigate the effects of various assumptions and the inclusion of different physical processes. This included the effects of including ion exchange, surface complexation and zeolites, using a larger reactive surface area, taking alternative thermodynamic data, and disregarding the effects of porosity change on the transport of species. Only a small set of the results obtained are discussed here in detail due to the limited space available; the full set of results are discussed in Watson *et al.* (2011). Here we concentrate on the role of ion exchange and surface complexation processes.

Model results

All of the modelling case results share similar characteristics and, broadly speaking, are able to replicate all the main features of the observed changes at the Tournemire site. Cases were run to 15 years, to match the length of time that the concrete had been in contact with the mudstone at Tournemire before the samples were taken.

Volume fraction plots of a 1.5 cm section around the concrete/mudstone interface are shown in Fig. 2 for cases with and without ion exchange and surface complexation. In each case, as expected, the mineralogical alteration is concentrated around the interface where the hyperalkaline leachate from the concrete mixes with the lower pH natural groundwater. The dissolution of portlandite releases Ca^{2+}, leading to an increase in calcite on both sides of the interface, particularly on the concrete side. Ettringite also precipitates around the interface, on the concrete side in the base case (as Al is released from dissolving aluminosilicates on the mudstone side and SO_4^{2-} levels increase due to the mudstone porewater diffusing into the concrete), and on the mudstone side as well when the extra processes of ion exchange and surface complexation are included.

The Ca/Si ratio in the concrete is decreased as the C-S-H gel solid solution shifts from a C-S-H$_{Jen}$ to C-S-H$_{Tob}$ endmember composition, caused by the inwards diffusion of aqueous silica from the dissolving minerals in the mudstone. The influx of silica and release of Ca from dissolving portlandite leads to an increase in the total amount of C-S-H gel within the concrete close to the interface, but there is no appearance of C-S-H in the mudstone which might be expected (and indeed was observed in the samples taken from Tournemire).

Within the mudstone, an increase in the amount of calcite present within the first 1 cm was predicted, and in the case with ion exchange and surface complexation a clear reaction front can be observed at 6 cm (0.5 cm from the concrete/ mudstone interface). The Mg-bearing minerals sepiolite and hydrotalcite precipitate in small amounts within the mudstone; these extend to a distance of approximately 2 cm from the interface. In the cases where zeolites were allowed to precipitate, gismondine (a Si-poor zeolite) also appears over a similar length scale.

Plots of the porosity profile at 0, 1, 5, 10 and 15 years are shown in Fig. 3 for the two cases. Away from the interface there is a slight increase in the porosity of the concrete and a slight decrease in that of the mudstone (again a reaction front at 6 cm is visible in profiles after 15 years). This is consistent with the findings of the recently published second Tournemire characterization study (Techer *et al.*, 2012). Pore blocking occurs at the interface itself, on the concrete side due to the precipitation of calcite and ettringite, and in the first compartment on the mudstone side in the later stages of the simulation due to the formation of ettringite (or calcite, in the base case). It is also clear from these plots that the region of intense mineralogical alteration is much smaller in the case where ion exchange and surface complexation are included.

The reason for this is clear when the pH profiles are examined (Fig. 4). In the base case, high pH levels (>10) extend over 10 cm from the interface, whereas when the extra processes are included the plume is restricted to less than 2 cm from the interface. The protonation/deprotonation reactions clearly contribute to the pH buffering capacity of the mudstone. The pH of the concrete porewater decreases slightly, to below 13 (from a starting pH of 13.4), whereas that of the mudstone porewater increases in the vicinity of the interface. Once the pore space is blocked, back-diffusion from the unaltered mudstone leads to a lowering of the pH near the interface.
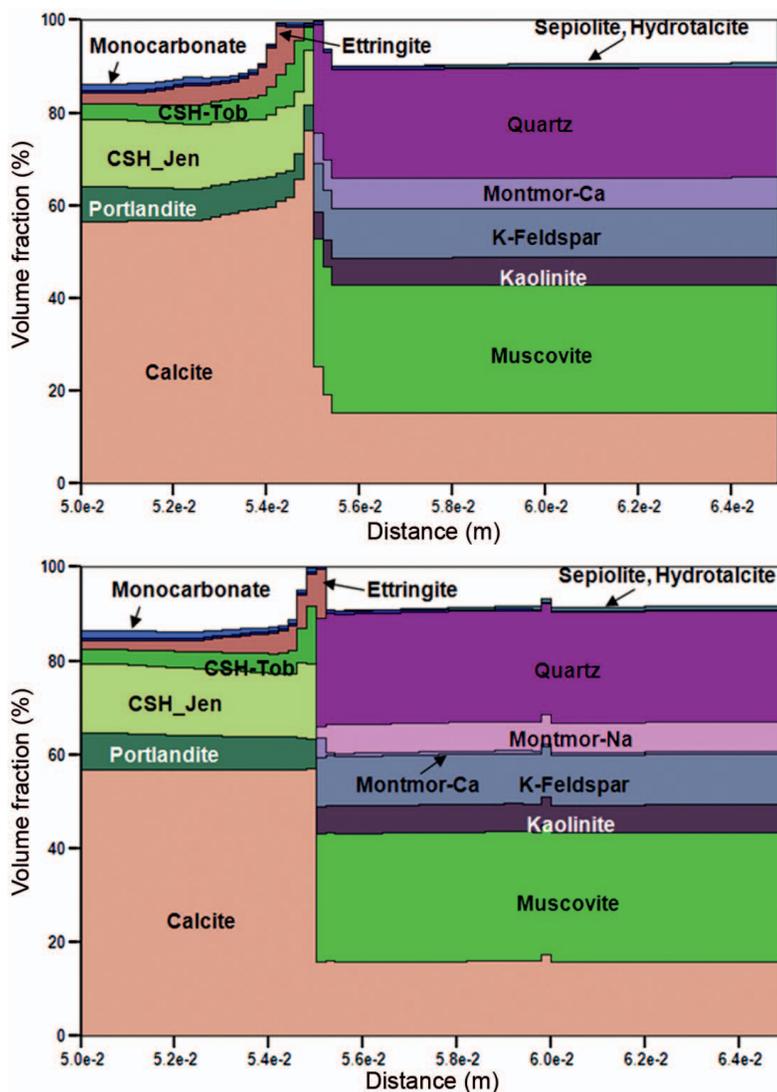
3451

FIG. 2. Volume fraction plots showing the mineral alteration after 15 years for cases with (bottom) and without (top) ion exchange and surface complexation. The concrete is on the left, the mudstone on the right.

Although not very clear in the volume fraction plots, the model also predicts dissolution of portlandite, and an increase in the C-S-H gel, calcite and ettringite content of the concrete near the interface, in agreement with the characterization studies. Calcite precipitates in the first 1−2 cm of the mudstone, and quartz and the clay minerals dissolve over the same spatial scale. There is also some limited K-feldspar overgrowth. The one area where the models do not match the experimental observations is in the growth of C-S-H gel within the mudstone itself. No C-S-H gel precipitated in the mudstone in any of the cases run. However, the predicted growth of zeolite (in cases where zeolites were included, results not shown here) may be taken as an analogue of the occurrence of C-A-S-H and thus provide some consistency with the mineralogical data (in the absence of thermodynamic data for C-A-S-H solids, low Al/Si zeolites such as stilbite and mordenite are the nearest analogue phase).
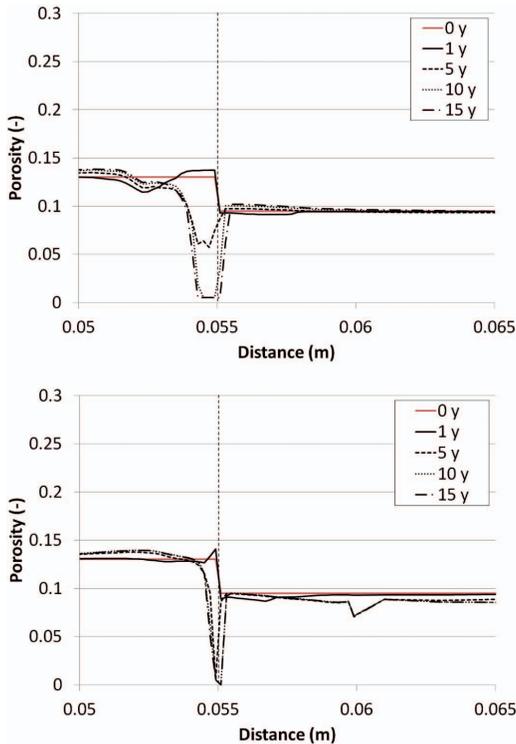
3452

FIG. 3. Porosity evolution around the interface for cases with (bottom) and without (top) ion exchange and surface complexation.
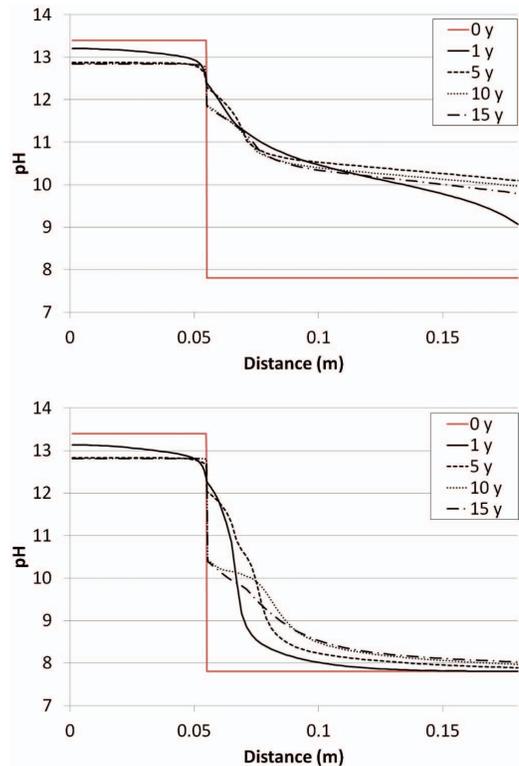

FIG. 4. Evolution of the pH plume profile for cases with (bottom) and without (top) ion exchange and surface complexation.

Conclusions

By studying the Tournemire industrial analogue as part of the LCS project we are able to build confidence in the predictive powers of our geochemical models. Each variant case was able to replicate all of the main features characterized by the laboratory studies of samples taken from the Tournemire site, with the exception of the precipitation of C-S-H gel observed at a depth of <1 cm in the mudstone. However, in the absence of thermodynamic data for C-A-S-H, the modelled presence of zeolite (in variant cases where zeolites were included) is consistent with this mineral acting as an analogue for the former and thus provides a reasonable fit with the mineralogical data. Despite this, a lack of quantitative data makes it difficult to assert that the predictions are a complete and true reflection of the evolution of the analogue. Nonetheless this exercise has been very useful in furthering our understanding of cement/rock interactions,

revealing that ion exchange and surface complexation processes (the latter in particular often neglected by modellers) have an important role in controlling the extent of the pH plume, especially in clay-dominated host rocks, or where clays are present in fracture fillings in crystalline rocks. Modelling an industrial analogue such as Tournemire provides an opportunity to model more complex processes (such as mineral growth) than those offered by laboratory systems, and as such can further our understanding and improve our models.

The LCS project is ongoing. Current activities include the further analysis of samples from the Maqarin natural analogue site at Jordan, and associated modelling tasks; the continuation of the *in situ* field test at the Grimsel underground laboratory, including monitoring of the hyper-alkaline plume resulting from injection of cementitious grout into boreholes intersected by fractures and the analysis of samples from a first overcoring exercise of one such borehole; and

3453

support of the Swiss National Fond Project on C-A-S-H data acquisition.

Acknowledgements

References

Baur, I., Keller, P., Mavrocordatos, D., Wehrli, B. and Johnson, C.A. (2004) Dissolution− precipitation behaviour of ettringite, monosulfate, and calcium silicate hydrate. *Cement and Concrete Research*, **34**, 341−348.

Beaucaire, C., Michelot, J.-L., Savoye, S. and Cabrera, J. (2008) Groundwater characterisation and modelling of water−rock interaction in an argillaceous formation (Tournemire, France). *Applied Geochemistry*, **23**, 2182−2197.

Bradbury, M.H. and Baeyens, B. (2003) Porewater chemistry in compacted re-saturated MX-80 bentonite. *Journal of Contaminant Hydrology*, **61**, 329−338.

Busenberg, E. and Plummer, L.N. (1982) The kinetics of dissolution of dolomite in CO_2-H_2O systems at 1.5 to 65ºC and 0 to 1 atm pCO_2. *American Journal of Science*, **282**, 45−78.

De Windt, L., Marsal, F., Tinseau, E. and Pellegrini, D. (2008) Reactive transport modeling of geochemical interactions at a concrete/argillite interface, Tournemire site (France). *Physics and Chemistry of the Earth*, **33**, S295−S305.

Gribi, P., Johnson, L.H., Suter, D., Smith, P.A., Pastina, B. and Snellman, M. (2008) *Safety Assessment for a KBS-3H Spent Nuclear Fuel Repository at Olkiluoto*. Process report, SKB R−08-36. Swedish Nuclear Fuel and Waste Management Company, Stockholm, Sweden.

Kline, W.E. and Fogler, H.S. (1981) Dissolution kinetics: the nature of the particle attack of layered silicates in HF. *Chemical Engineering Science*, **36**, 871−884.

Kulik, D.A. and Kersten, M. (2001) Aqueous solubility diagrams for cementitious waste stabilization systems: II, end-member stoichiometries of ideal calcium silicate hydrate solid solutions. *Journal of the American Ceramic Society*, **84**, 3017−3026.

Lasaga, A.C. (1998) *Kinetic Theory in the Earth Sciences*. Princeton University Press, Princeton, New Jersey, USA, 811 pp.

Lothenbach, B. and Winnefeld, F. (2006) Thermodynamic modelling of the hydration of Portland cement. *Cement and Concrete Research*, **36**, 209−226.

Lothenbach, B., Matschei, T., Moschner, G. and Glasser, F.P. (2008) Thermodynamic modelling of the effect of temperature on the hydration and porosity of Portland cement. *Cement and Concrete Research*, **38**, 1−18.

Mao, L. (2010) Dissolution kinetics of scolecite in alkaline environments. *Reinvention: a Journal of Undergraduate Research*, **2**.

Matschei, T., Lothenbach, B. and Glasser, F.P. (2007) Thermodynamic properties of Portland cement hydrates in the system $CaO-Al_2O_3-SiO_2-CaSO_4-CaCO_3-H_2O$. *Cement and Concrete Research*, **37**, 1379−1410.

Palandri, J.L. and Kharaka, Y.K. (2004) *A Compilation of Rate Parameters of Water−Mineral Interaction Kinetics for Application to Geochemical Modelling*. USGS Open File Report 2004-1068. United States Geological Survey, Menlo Park, California, USA.

Plettinck, S., Chou, L. and Wollast, R. (1994) Kinetics and mechanisms of dissolution of silica at room temperature and pressure. V.M. Goldschmidt Abstracts, Edinburgh. *Mineralogical Magazine*, **58A**, 728−729.

Sato, T., Kuroda, M., Yokoyama, S., Tsutsui, M., Fukushi, K., Tanaka, T. and Nakayama, S. (2004) Dissolution mechanism and kinetics of smectite under alkaline conditions. Pp. A3-38−A3-46 in: *International Workshop on Bentonite−Cement Interaction in Repository Environments* (R. Metcalfe and C. Walker, editors). NUMO/Posiva, Tokyo, Japan.

Savage, D., Cave, M.R., Haigh, D., Milodowski, A.E. and Young, M.E. (1993) The reaction kinetics of laumontite under hydrothermal conditions. *European Journal of Mineralogy*, **5**, 523−535.

Savage, D., Rochelle, C.A., Moore, Y., Milodowski, A., Bateman, K., Bailey, D. and Mihara, M. (2001) Analcime reactions at 25−90ºC in hyperalkaline fluids. *Mineralogical Magazine*, **65**, 571−587.

Savage, D., Benbow, S., Watson, C., Takase, H., Ono, K., Oda, C. and Honda, A. (2010) Natural systems evidence for the alteration of clay under alkaline conditions: an example from Searles Lake, California. *Applied Clay Science*, **47**, 72−81.

Savage, D., Soler, J.M., Yamaguchi, K., Walker, C., Honda, A., Inagaki, M., Watson, C., Wilson, J., Benbow, S., Gaus, I. and Rueedi, J. (2011) A comparative study of the modelling of cement hydration and cement-rock laboratory experiments. *Applied Geochemistry*, **26**, 1138−1152.

Smellie, J.A.T., Alexander, W.R., Degnan, P., Griffault, L., Mäder, U. and Trotignon, L. (2001) The role of

the Jordan natural analogue studies in the performance assessment of cementitious repositories for radioactive wastes. Pp. 1391−1393 in: *Water−Rock Interaction 10* (R. Cidu, editor). A.A. Balkema, Leiden, The Netherlands.

Soler, J.M. and Mäder, U.K. (2007) Mineralogical alteration and associated permeability changes induced by a high-pH plume: modeling of a granite core infiltration experiment. *Applied Geochemistry*, **22**, 17−29.

Soler, J.M., Paris, B., Pfingsten, W. and Mäder, U. (2004) Flow and reactive transport modeling in the framework of GTS-HPF. Pp. 983−987 in: *Water−Rock Interaction 11* (R.B. Wanty and R.R. Seal, editors). A.A. Balkema, Leiden, The Netherlands.

Techer, I., Bartier, D., Boulvais, Ph., Tinseau, E.,

Suchorski, K., Cabrera, J. and Dauzères, A. (2012) Tracing interactions between natural argillites and hyper-alkaline fluids from engineered cement paste and concrete: Chemical and isotopic monitoring of a 15-years old deep-disposal analogue. *Applied Geochemistry*, **27**, 1384−1402.

Tinseau, E., Bartier, D., Hassouta, L., Devol-Brown, I. and Stammose, D. (2006) Mineralogical characterization of the Tournemire argillite after *in situ* reaction with concretes. *Waste Management*, **26**, 789−800.

Watson, C., Savage, D., Wilson, J. and Walker, C. (2011) *Reactive Transport Modelling of the Tournemire Analogue*. Quintessa report for the UK Nuclear Decommissioning Authority, QRS-1523A-1.